

The distribution of inelastic dark matter in the Sun

Mattias Blennow,^{1,2,*} Stefan Clementz,^{1,†} and Juan Herrero-Garcia^{3,‡}

¹*Department of Physics, School of Engineering Sciences, KTH Royal Institute of Technology, AlbaNova University Center, 106 91 Stockholm, Sweden*

²*Instituto de Física Teórica UAM/CSIC, Calle Nicolás Cabrera 13-15, Cantoblanco E-28049 Madrid, Spain*

³*ARC Center of Excellence for Particle Physics at the Terascale (CoEPP), University of Adelaide, Adelaide, SA 5005, Australia*

Abstract

If dark matter is composed of new particles, these may be gravitationally bound to the Sun after scattering on solar nuclei, thermalize after further interactions, and finally annihilate into Standard Model particles, generating neutrinos which we can detect on Earth. Typically, one assumes that equilibration between capture and annihilations has been reached, so that the annihilation rate is completely determined by the capture rate. For elastic interactions, this is usually an excellent approximation, while it may not be so for dark matter scattering inelastically into a slightly heavier ($\mathcal{O}(10 - 100)$ keV) state. One issue is that the kinetic energy of the captured dark matter, after having scattered a number of times, might not be sufficient to allow up-scattering, at which point the thermalization process effectively stops. Moreover, down-scatterings from the excited state may cause a large evaporation rate. In this work we perform a numerical simulation of the whole process in order to check: if the distribution reaches a stationary state in a solar lifetime; if thermalization with solar nuclei occurs, i.e., if the final distribution is isothermal (Maxwell-Boltzmann); in case the distribution is not isothermal, whether the annihilation rate into neutrinos is sizeable, and the conditions under which equilibrium between annihilation and capture is reached are satisfied; and finally, whether evaporation plays an important role. We find that, unless the mass splitting is very small ($\lesssim 50$ keV) and/or the dark matter has a sub-dominant elastic cross section, the dark matter distribution does not reach a stationary state, it is not isothermal at the solar temperature, annihilations are suppressed and equilibration is not reached. We also find that evaporation induced by down-scattering is not effective in reducing the total dark matter abundance.

*Electronic address: m.blennow@csic.es

†Electronic address: scl@kth.se

‡Electronic address: juan.herrero-garcia@adelaide.edu.au

I. INTRODUCTION

A popular class of models for explaining a number of observations in astrophysical systems is that of particle dark matter (DM) [1–4]. In the event that DM interacts with the particles of the standard model (SM), many different methods for observing it have been proposed, followed by a number of experiments that have been able to place impressive bounds on its mass and interaction cross section.

One of the many ways of searching for DM is to look for the effects that it may have on the Sun as it is captured by scattering against solar material [5–7]. A large population of captured DM may have two observable effects on the Sun. If DM annihilates (e.g., thermal relics), SM particles can be produced that in turn decay or otherwise interact to give rise to a flux of high energy neutrinos that can be searched for in neutrino telescopes on Earth. Searches of this type have been performed by various collaborations [8–11]. The accumulation of large amounts of DM in the Sun may also affect helioseismology and the solar temperature, which can potentially lead to observational effects with the possibility to constrain DM properties or alleviate the solar composition problem [12–26].

A type of DM model that can possibly be probed by the production of neutrinos from DM annihilations inside the Sun is that of inelastic DM [27]. These models were originally introduced to reconcile the observation of the DAMA/LIBRA experiment [28] as it was ruled out, if due to a standard elastically scattering DM particle, by the CDMS experiment [29], which is now joined by a number of other experiments including the large Xenon-based experiments LUX [30], PandaX [31], and XENON [32]. It should also be mentioned that it is difficult to reconcile DAMA with other direct detection experiments also for inelastic DM [33]. The evasion of the bounds from CDMS came from the introduction of a small mass splitting δ that separated two different DM states which upon scattering change from one to the other. In the scattering process, some energy was converted from kinetic energy to mass, which gave this type of models its name. The introduced mass splitting has a large impact on the scattering kinematics of DM and translates into altered solar capture rates of inelastic DM. The inelastic DM capture in the Sun has been discussed for both the cases of endothermic and exothermic reactions in, e.g., Refs. [34–39]. See also Refs. [40–42] for studies of inelastic DM capture by compact stars such as white dwarves and neutron stars. Inelastic DM with large self-interactions has also been proposed as a solution to the small scale structure problems [43–45].

Upon being captured inside the Sun, DM is often assumed to instantaneously thermalize with the surrounding plasma, in which case its number density distribution is well described by a

Boltzmann distribution with a specific temperature, i.e., $f \sim \exp(-E/T)$. This has been the assumption also in the case where the capture of inelastic DM by the Sun has been studied. However, if δ is comparable to the kinetic energy of DM particles as they fall into the Sun, large energies are required in a collision in order for up-scattering to occur. This implies that the DM particles scatter only off high velocity (and thus Boltzmann suppressed) solar nuclei, so that the probability for scattering is very small, or that their orbit takes them from a radius with a large gravitational potential, which provides the necessary kinetic energy, into regions closer to the solar center. Moreover, when a DM particle subsequently down-scatters, it may be boosted by the significant amount of energy that is released to such a velocity that it is no longer gravitationally bound. With this in mind, it is not obvious that a thermalized distribution is to be expected in the case of inelastic DM, nor is it clear if and when evaporation has to be taken into account. Both of these phenomena can have an impact on the annihilation rate of captured DM. A non-thermal distribution could alter the annihilation rate so that a larger population of DM must be present in order for equilibrium between solar capture and annihilation to take place, while evaporation would reduce the total number of particles that can annihilate. The assumption of capture-annihilation equilibrium allows one to bypass the annihilation rate in favour of a direct link between neutrino rates and the solar capture rate. Due to the effects of inelastic scattering on the annihilation rate, it is unclear if this is a justified assumption.

In this paper, we will study the thermalization process of inelastic DM using simulations and the impact that inelastic scattering has on the annihilation and evaporation rates. In Sec. II, we discuss the inelastic DM framework and the relevant kinematic effects introduced by a mass splitting. In Sec. III, we describe our approach to the problem and the numerical implementation of the simulation. The results are presented and discussed in Sec. IV. Finally, we summarize and give our conclusions in Sec. V.

II. INELASTIC DARK MATTER

There are various scenarios in which inelastic DM appears naturally [46–48]. In the simplest models, inelastic DM consist of two states χ and χ^* , with masses $m_\chi < m_{\chi^*}$ that satisfy

$$m_{\chi^*} - m_\chi = \delta \ll m_\chi. \quad (1)$$

Although the mass splitting is very small relative to the DM masses, it has a significant impact on the resulting differential rates in direct detection (DD) experiments, as was noted in Ref. [27].

According to our definition of the DM masses, χ^* is the slightly more massive state, which indicates that the scattering process is endothermic when the incoming DM particle is a χ and exothermic when the incoming particle is a χ^* . Below, we will discuss the endothermic case. The case of exothermic scattering can be recovered by substituting $\delta \rightarrow -\delta$.

We will primarily study inelastic DM that interacts with protons and neutrons through spin-independent operators. This is due to the fact that spin-dependent interactions in the Sun takes place primarily between DM and protons. Even though capture of χ^* originating from the halo due to exothermic scattering can be large for a spin-dependent cross section [22], given the very low mass of protons compared to the DM that we consider, scattering from the lower to the higher mass state is essentially forbidden due to kinematics, unless the mass splitting is so small that it is no longer interesting. These particles would thus never thermalize but the Sun would be surrounded by a cloud of loosely bound DM, composed entirely of the lower mass state, that would never scatter again. We will focus on the case in which the galactic halo is composed of both χ and χ^* with equal abundances. This is plausibly the case, as the temperature at which the overall DM abundance freeze-out occurs is of the order $m_\chi/20$, which far exceeds δ .

A. Scattering kinematics

The scattering kinematics of DM is extensively covered in Ref. [38]. We will here shortly review the scattering kinematics that will be important for the discussions that follow.

When DM scatters inelastically, the only modification to the cross section with respect to the elastic case is a multiplying phase-space factor. If the elastic DM–nucleus scattering cross section is σ_0 , then the inelastic scattering cross section σ_{inel} would be

$$\sigma_{\text{inel}} = \sqrt{1 - \frac{2\delta}{\mu_{\chi A} v_{\text{rel}}^2}} \sigma_0, \quad (2)$$

where v_{rel} is the relative speed between the DM particle and its target, and $\mu_{\chi A}$ is the DM–target reduced mass. When DM scatters endothermically, the relative velocity between the DM particle and its target must exceed

$$u_{\text{rel,lower}} = \sqrt{2\delta/\mu_{\chi A}}, \quad (3)$$

or there will simply not be enough kinetic energy to produce the mass required for the heavier state. On the other hand, there is no such constraint for exothermic scattering, as it is always kinematically allowed.

When a collision occurs, the solution to the energy and momentum conservation equations yields the largest, E_{\max} , and the smallest, E_{\min} , recoil energy of the target solar nucleus

$$E_{\max(\min)} = 2 \frac{\mu_{\chi A}^2}{m_\chi m_A} E_{i,\text{kin}} \left(1 (\pm) \sqrt{1 - \frac{m_\chi}{\mu_{\chi A} E_{i,\text{kin}}} \delta} \right) - \frac{\mu_{\chi A}}{m_A} \delta, \quad (4)$$

where m_A is the mass of the target nucleus, and $E_{i,\text{kin}} = E_i - \phi(r)$ is the kinetic energy of the incoming DM particle. The allowed range of recoil energies E_R for a given $E_{i,\text{kin}}$ will be in the range $E_{\min} \leq E_R \leq E_{\max}$.

In order for an inelastic DM particle to give rise to a specific recoil energy in a collision, its velocity must be larger than

$$v_m^2 = \left(\sqrt{\frac{m_A E_R}{2\mu^2}} + \frac{\delta}{\sqrt{2m_A E_R}} \right)^2. \quad (5)$$

Unlike elastic DM, the maximum rate for inelastic DM scattering in a DD experiment will be at a non-zero recoil energy. Namely, the mass splitting induces a shift of the rate towards the recoil energy that minimizes v_m , implying that experiments may miss the detection of inelastic DM simply due to not searching in a large enough energy range, as briefly mentioned in Ref. [38] and thoroughly studied in Ref. [49].

In the rest frame of the target nuclei, the angle θ between the velocity vectors of the incoming and outgoing DM particle satisfy

$$\cos(\theta) = \frac{E_{i,\text{kin}} + E_{f,\text{kin}} - m_A E_R / m_\chi}{2\sqrt{E_{i,\text{kin}} E_{f,\text{kin}}}}, \quad (6)$$

where $E_{f,\text{kin}} = E_f - \phi(r)$ is the kinetic energy of the outgoing DM particle. This relation will be needed to determine the change of trajectory of a DM particle as it scatters.

III. SOLAR CAPTURE, THERMALIZATION, AND ANNIHILATION

The method we will employ to investigate the thermalization of inelastic DM is similar to that of Refs. [50, 51]. This section presents the implementation of the numerical simulation.

A. The phase space evolution of a captured population

The effective Hamiltonian \mathcal{H} describing a particle moving in a central potential $\phi(r)$ is given by

$$\mathcal{H} = m_\chi E = \frac{1}{2} m_\chi \dot{r}^2 + \frac{m_\chi L^2}{2r^2} + m_\chi \phi(r) \equiv \frac{1}{2} m_\chi \dot{r}^2 + m_\chi V_{\text{eff}}(L, r). \quad (7)$$

It is also very convenient, as we have done, to define the reduced energy E as the energy divided by the DM mass, as well as the reduced angular momentum $\vec{L} = \vec{r} \times \vec{v}$, given the fact that the orbit of a particle in a central potential is independent of its mass. Since E and $L = |\vec{L}|$ are conserved quantities, it is convenient to describe the DM particle orbit by these quantities rather than position and velocity.¹ For a given an angular momentum L , the smallest energy $E_{\min}(L)$ of a particle with a trajectory that intersects the Sun will be given by

$$E_{\min}(L) = \min_{r \leq R_{\odot}} V_{\text{eff}}(L, r). \quad (8)$$

Taking the above into consideration, we find it convenient to define the combination $\alpha = (E, L)$ as a label for the position in phase space of a particular DM particle.

The time evolution of the total number of captured DM particles $N(t)$ follows the differential equation

$$\dot{N} = C_{\odot} - E_{\text{evap}} - \Gamma_{\text{ann}}, \quad (9)$$

where $\dot{N} \equiv dN/dt$, C_{\odot} is the solar capture rate, E_{evap} , which is proportional to N , is the evaporation rate and Γ_{ann} , which is proportional to N^2 , is the rate at which particles are annihilated.² If evaporation is neglected, the equilibrium solution ($\dot{N} = 0$) of the evolution equation reads

$$C_{\odot} = \Gamma_{\text{ann}}, \quad (10)$$

which implies that there is equilibrium between capture and annihilations. In order to rigorously test this condition, one must calculate the annihilation rate. However, this requires knowledge of how the DM is distributed in the Sun. In our simulations, the distribution of particles is discretized in E and L such that f_{α} describes the number of particles in a particular state α . The evolution of the distribution is then governed by the equation

$$\dot{f}_{\alpha} = \sum_{\beta} \Sigma_{\alpha\beta} f_{\beta} + C_{\alpha} - f_{\alpha} \sum_{\beta} \Gamma_{\alpha\beta} f_{\beta}. \quad (11)$$

Each element in \vec{f} contains the total number of particles in state α , while each element in \vec{C} gives the capture rate into the corresponding state. The off-diagonal elements in $\Sigma_{\alpha\beta}$ ($\alpha \neq \beta$) give the rate with which particles in state β scatter against solar nuclei and end up in the state α . The

¹ We assume spherical symmetry, i.e., orbits in different planes are equivalent. We will therefore only use L , the total magnitude of \vec{L} , and not its 3 components.

² Note that in the literature the last term is often written as $2\Gamma_{\text{ann}}N^2$. In this work we absorb the factor of 2 into Γ_{ann} and use a differently normalized number density distribution function.

diagonal entries in Σ are negative and correspond to the rate at which particles scatter from the corresponding state to all other states, including evaporation, i.e., positive energy states where the DM particle escapes the Sun's gravitational well. Finally, $\Gamma_{\alpha\beta}$ gives the rate at which a particle in state α annihilates with a particle in state β .³

We also need to know the fraction of the time that a particle in a given state α finds itself at a radius r as it travels between the maximal radius, r_+ , and the minimal radius, r_- , of the complete orbit, that are found by solving Eq. (7) with the substitution $\dot{r} = 0$. The time it takes the particle to move between radius r_1 to radius r_2 can be found by isolating \dot{r} in Eq. (7) and solving the differential equation, which leads to

$$T(r_1, r_2) = \int dt = \int_{r_1}^{r_2} \frac{dr}{\dot{r}} = \int_{r_1}^{r_2} \frac{dr}{\sqrt{2(E - V_{\text{eff}}(L, r))}}. \quad (12)$$

Integrating from $r_1 = r_-$ to $r_2 = r_+$ gives the time for a particle to complete half an orbit.

B. Solar capture

The derivation of the solar capture rate of DM particles originating from the DM halo dates back several decades [5, 7]. In the standard calculation, any information on the DM energy and angular momentum post scattering is discarded since any particle with $E < 0$ is counted towards the total capture. However, we are not only interested in the total capture rate but also in the distribution of the captured particles in $E - L$ space. We therefore give a short description of how we compute C_α .

The solar capture rate of DM is, in differential form, given by [7]

$$dC = \pi n_\chi \frac{f(u)}{u} \frac{d\sigma}{dE_R}(w, E_R) n_A(r) \frac{2}{\sqrt{1 - (L/rw)^2}} dr du dE_R dL^2. \quad (13)$$

In the above, we have assumed that the target nuclei is stationary, r is the radius at which scattering occurs, $n_A(r)$ is the local density of target particles of species A , u is the DM velocity at a distance where the gravitational potential of the Sun is negligible, and $w = \sqrt{u^2 + v_{\text{esc}}(r)^2}$ is the velocity of the particle at radius r . The local halo number density of DM and its speed distribution at the location of the Sun explicitly enter as n_χ and $f(u)$. Note that the velocity distribution $\tilde{f}(\vec{u})$ is normalized so that

$$\int \tilde{f}(\vec{u}) d^3u = \int f(u) du = 1, \quad (14)$$

³ In the case of DM self-capture due to self-interactions, see e.g., Ref. [52], $\Sigma_{\alpha\beta}$ would also incorporate that effect.

where

$$f(u) = \int \tilde{f}(u, \theta, \phi) u^2 \sin(\theta) d\theta d\phi. \quad (15)$$

The quantity L^2 is the square of the reduced angular momentum of the incoming DM particle from the DM halo and $d\sigma/dE_R(w, E_R)$ is the differential cross section [27]

$$\frac{d\sigma}{dE_R}(w, E_R) = \frac{m_A A^2 \sigma_{\chi p}}{2\mu_{\chi p}^2 w^2} |F(E_R)|^2. \quad (16)$$

Here it has been assumed that the coupling between DM and nuclei is isospin conserving, leading to the A^2 enhancement of the cross section, where A is the total number of nucleons.⁴ Furthermore, $\sigma_{\chi p}$ is the DM–proton cross section entering as σ_0 in Eq. (2), $\mu_{\chi p}$ is the DM–proton reduced mass, and w is the relative velocity between the DM and the nucleus. Interestingly, the phase-space factor relating the inelastic and elastic scattering cross sections in Eq. (2) is cancelled. The form factor $F(E_R)$ accounts for the decoherence in the DM–nucleus scattering process when the momentum transfer q , which relates to E_R as $q = \sqrt{2m_A E_R}$, is large.

In order to calculate C_α , the integral in Eq. (13) is discretized over the integration region. The limits in r and L^2 are $0 < r < R_\odot$, which is the solar radius, and $0 < L^2 < r^2 w^2$, respectively. The limits in u and E_R are complicated and we refer to the discussion in Ref. [38]. At each discretization point, the incoming DM velocity vector \vec{w}_i can be reconstructed. When the DM particle scatters, its energy post-collision is known from

$$E_f = E_i - E_R - \delta/m_\chi, \quad (17)$$

where $E_{i(f)}$ is the energy of the incoming (outgoing) DM particle. The outgoing DM speed w_f is known from the equation above. The angle θ between the incoming and outgoing velocity vector is given by Eq. (6). There is also an azimuthal angle φ around \vec{w}_i at which the outgoing velocity vector lies that is randomly distributed in the interval 0 to 2π . In terms of these angles the radial distance r , the angular momentum of the outgoing DM particle L_f is given by

$$L_f^2 = r^2 w_f^2 \left[1 - \left(\sqrt{1 - \left(\frac{L}{r w} \right)^2} \cos(\theta) - \frac{L}{r w} \sin(\theta) \cos(\varphi) \right)^2 \right]. \quad (18)$$

Using Monte-Carlo methods, we find the probability distribution for a scattering DM particle at each discretization point to end up in a state α . Finally, \vec{C} is found by summing over all discretized states weighted by their probability densities.

⁴ For isospin violating DM, A^2 is instead replaced by the factor $(Z + (A - Z)f_n/f_p)^2$, where Z is the number of protons and f_p (f_n) is the coupling of DM to protons (neutrons).

C. Scattering among different states

When DM particles have been captured, occasional scattering with solar nuclei will take a particle initially in the $\beta = (E_i, L_i)$ state into the state $\alpha = (E_f, L_f)$. The differential scattering rate at radius r of a DM particle with velocity $\vec{w}(r)$, travelling through a gas of nuclei of element A with velocity \vec{v} , number density $n_A(r)$, and velocity distribution $f_A(r, \vec{v})$, is given by [50]

$$dR(r) = \sigma n_A(r) f_A(r, \vec{v}) |\vec{w}(r) - \vec{v}| d^3v, \quad (19)$$

where the velocity distribution of the nuclei is a Boltzmann distribution

$$f_A(r, \vec{v}) = \left(\frac{m_A}{2\pi T(r)} \right)^{3/2} \exp\left(-\frac{m_A \vec{v}^2}{2T(r)} \right), \quad (20)$$

and $T(r)$ is the temperature of the solar plasma at radius r . The cross section σ that enters will be the integral over the differential cross section in the frame in which the nucleon is stationary.

In order to find $\Sigma_{\alpha\beta}$, we discretize the Sun into thin shells at radii r_i . Under the assumption that particles complete many orbits between interactions, the rate at which particles in state β scatter at radius r_i and end up in state α is given by

$$\mathcal{R}_{\beta\rightarrow\alpha}(r_i) = R_\beta(r_i) \mathcal{T}_\beta(r_i) \mathcal{P}_{\beta\rightarrow\alpha}(r_i). \quad (21)$$

In the above, $R_\beta(r_i)$ is the total scattering rate at radius r_i and $\mathcal{T}_\beta(r_i)$ is the fraction of the orbital time that the particle spends inside the shell. The factor $\mathcal{P}_{\beta\rightarrow\alpha}(r_i)$ is the probability that the particle ended up in the particular state α after it scattered at r_i . Having calculated the above, the off-diagonal elements in the Σ matrix are given by the sum of contributions from all shells that the particle passes through on its orbit

$$\Sigma_{\alpha\beta} = \sum_i \mathcal{R}_{\beta\rightarrow\alpha}(r_i). \quad (22)$$

The diagonal elements of the Σ matrix are given by the negative of the total scattering rate from state α ,

$$\Sigma_{\alpha\alpha} = - \sum_i R_\alpha(r_i), \quad (23)$$

which also includes evaporation.

To find $\mathcal{P}_{\beta\rightarrow\alpha}(r)$, the DM velocity vector \vec{w}_i of a particle in state $\beta = (E_i, L_i)$ before scattering is required. In the Sun's rest frame, the magnitude is found to be

$$w_i(r) = \sqrt{2E_i - 2\phi(r)}. \quad (24)$$

We are free to choose a coordinate system in which $\vec{r} = (r, 0, 0)$. The angle between \vec{r} and $\vec{w}_i(r)$ is given by $\xi = \sin^{-1}(L_i/rw_i(r))$ with which the DM velocity vector is given by

$$\vec{w}_i(r) = w_i(r) (c_\xi, s_\xi, 0), \quad (25)$$

where we use the notation $s_x = \sin(x)$, and $c_x = \cos(x)$. The velocity vector of the nucleus can be parametrized in terms of two other angles η and φ_1 as

$$\vec{v} = v (c_\xi c_\eta - s_\xi s_\eta c_{\varphi_1}, s_\xi c_\eta + c_\xi s_\eta c_{\varphi_1}, s_\eta s_{\varphi_1}), \quad (26)$$

where the angles η and φ_1 are uniformly distributed in the intervals $0 < \eta < \pi$ and $0 < \varphi_1 < 2\pi$, respectively. We have chosen the nuclei and DM velocity vectors to be aligned if $\eta = 0$.

If scattering is possible, a Galilean transformation is made to the frame in which the nucleus is stationary and the DM velocity is $\vec{w}_{i,\text{sc}} = \vec{w}_i(r) - \vec{v}$. It is in this reference frame that the recoil energy E_R is defined and its allowed range is in the interval $[E_{\min}, E_{\max}]$, given by Eq. (4). For a given recoil energy, the angle θ between the outgoing DM velocity $\vec{w}_{f,\text{sc}}$ and $\vec{w}_{i,\text{sc}}$ can be calculated using Eq. (6). Transforming back to the Sun's rest frame, the DM velocity after scattering is

$$\vec{w}_f = \mathcal{R}(\varphi_2)\vec{w}_{f,\text{sc}} + \vec{v}, \quad (27)$$

where the operator $\mathcal{R}(\varphi_2)$ rotates $\vec{w}_{f,\text{sc}}$ around $\vec{w}_{i,\text{sc}}$ by the angle φ_2 , which is uniformly distributed in the interval $0 < \varphi_2 < 2\pi$. The state in which the DM particle ends up in is given by

$$E_f = E_i + \frac{1}{2} (w_f^2 - w_i^2(r)), \quad L_f^2 = r^2 w_f^2 - (\vec{r} \cdot \vec{w}_f)^2. \quad (28)$$

The fractional time spent in the shell with inner radius r_{inner} and outer radius r_{outer} is calculated as

$$\mathcal{T}_\beta(r_i) = \frac{T(r_{\text{inner}}, r_{\text{outer}})}{T(r_-, r_+)}, \quad (29)$$

where $T(r_1, r_2)$ is given in Eq. (12). The shell widths are chosen so that

$$r_{\text{inner}} = \frac{r_{i-1} + r_i}{2}, \quad r_{\text{outer}} = \frac{r_i + r_{i+1}}{2}. \quad (30)$$

The $\Sigma_{\alpha\beta}$ matrix is then found using Monte-Carlo methods.

D. The radial number distribution function and the annihilation rate

To calculate the annihilation rate of DM, a detailed knowledge of the radial number density distribution function $f(r)$ is necessary. The annihilation rate for self-annihilating DM is given by

$$\Gamma_{\text{ann}} = \int \sigma_{\text{ann}}(\vec{v}_{\text{rel}}) |\vec{v}_{\text{rel}}| f(\vec{r}, \vec{v}_1) f(\vec{r}, \vec{v}_2) d^3 v_1 d^3 v_2 d^3 r, \quad (31)$$

where $\vec{v}_{\text{rel}} = \vec{v}_1 - \vec{v}_2$ is the relative velocity between the two colliding particles and $f(r, \vec{v})$ is the phase-space density distribution for DM, which has been normalized so that

$$\int f(\vec{r}, \vec{v}) d^3v d^3r = N, \quad (32)$$

where N is the total number of captured DM particles. We will assume that the spatial distribution is spherically symmetric. However, a possible consequence of a very low number of scattering events of a particle over a long time may be a preference for some orbital planes over others due to a directional dependence of the flux of incoming DM particles. Such a directional dependence could be caused by, for example, the solar motion through the DM halo or anisotropies in the galactic velocity distribution of DM. This would introduce an angular dependence in the the number density distribution so that the local DM distribution is increased in some regions relative to the spherically symmetric case, which would increase the overall annihilation rate. However, we will assume that spatial spherical symmetry holds when evaluating Eq. (31), keeping in mind the discussion above.

When the mean free path of DM inside the Sun is much larger than the solar radius (as is considered here), the radial number density distribution is often approximated as an isothermal Maxwell-Boltzmann distribution that can be written as [6, 12, 22, 52–54],

$$f_{\text{iso}}(\vec{r}) = n_0 \exp(-\vec{r}^2/r_\chi^2) N, \quad (33)$$

where $n_0 = \pi^{-3/2} r_\chi^{-3}$. The length scale r_χ of the distribution is, assuming constant solar density and temperature, given by

$$r_\chi^2 = \frac{3k_B T_c}{2\pi G \rho_c m_\chi}, \quad (34)$$

where k_B is the Boltzmann constant and G is the gravitational constant. The bulk of the DM distribution is generally located in such a centralized region that the density ρ_c and temperature T_c can be approximated by the corresponding values at the Sun's center. For elastic DM, this assumption is generally valid for scattering cross sections that yield significant capture rates, see e.g., Refs. [55, 56]. In this case, the annihilation rate of DM, written in terms of the thermal averaged annihilation cross section $\langle \sigma_{\text{ann}} v \rangle$, is

$$\Gamma_{\text{ann,iso}} = \langle \sigma_{\text{ann}} v \rangle \int f_{\text{iso}}^2(\vec{r}) d^3r. \quad (35)$$

It is clear that altering $f(\vec{r}, \vec{v})$ can significantly modify the expected annihilation rate, and such a change is expected for inelastic DM if the sub-dominant elastic scattering is negligible. As our simulated distributions will be given in E - L space, we must map them onto r - v space. With

the assumption of many orbits per scattering, a DM particle in state α will spend the fractional time $\mathcal{T}_\alpha(r)$ at radius r . The radial distribution function can thus be calculated by distributing all particles of each state into all possible radii, weighed by the fractional time spent at that radii:

$$\tilde{f}_{\text{num}}(r) = \sum_{\alpha} f_{\alpha} \mathcal{T}_{\alpha}(r). \quad (36)$$

This is just the angular averaged distribution of the full three-dimensional spatial distribution, i.e.,

$$\tilde{f}_{\text{num}}(r) = r^2 \int f_{\text{num}}(r, \theta, \varphi) \sin(\theta) d\theta d\phi. \quad (37)$$

Since spherical symmetry has been assumed, the relation above informs us that the three-dimensional distribution function $f(\vec{r})$ can be found from $\tilde{f}(r)$ as $f_{\text{num}}(\vec{r}) = (4\pi r^2)^{-1} \tilde{f}_{\text{num}}(r)$. Unfortunately, solving Eq. (11) to find f_{α} can be computationally infeasible. Neglecting the annihilation rate, the analytic solution for \vec{f} is

$$\vec{f}(t) = \int_0^t e^{\Sigma(t-t')} \vec{C}(t') dt', \quad (38)$$

where a possible time-dependence in the solar capture rate has been taken into account. This will allow us to find out if the total capture of DM is in equilibrium with the loss due to evaporation after a solar lifetime. It will also allow us to calculate the annihilation rate, and compare it with that of an isothermal distribution.

The annihilation cross section times relative velocity can be expanded as

$$\sigma(v_{\text{rel}})v_{\text{rel}} = a + bv_{\text{rel}}^2 + \dots \quad (39)$$

where a is non-zero for s-wave annihilation. We will make a simple comparison of s-wave annihilating DM from a Boltzmann distribution to the distribution that we extract from our numerical data. Since the relative velocities of DM particles in the Sun are small, if both $a, b \neq 0$, a will dominate and $\sigma(v_{\text{rel}})v_{\text{rel}}$ will be constant. In this case, we can trivially calculate the integrals over \vec{v}_1 and \vec{v}_2 in Eq. (31) and find the ratio of the s-wave annihilation rate for the derived distribution

$$\Gamma_{\text{ann,num}}(t) = \langle \sigma_{\text{ann}} v \rangle \int f_{\text{num}}^2(\vec{r}, t) d^3r, \quad (40)$$

and the isothermal distribution in Eq. (35), that is

$$\frac{\Gamma_{\text{ann,num}}(t)}{\Gamma_{\text{ann,iso}}} = \frac{\int f_{\text{num}}^2(\vec{r}, t) d^3r}{\int f_{\text{iso}}^2(\vec{r}) d^3r}. \quad (41)$$

This provides us with a quantitative measure of how much the annihilation rate is affected due to the scattering being inelastic.

Note that if the annihilation cross section is velocity dependent, one needs the full phase-space distribution. Under the assumption of a spherical distribution, it can be found as follows. Any state that contributes to $\tilde{f}(r)$ at some radius r will give a contribution to the velocity distribution at this radius. The magnitude of the velocity v can be found in Eq. (24), while the angle between the radial coordinate and the velocity vector is $\psi_1 = \sin^{-1}(L/r_iv)$. These two relations can be used to extract the two-dimensional velocity distribution $f(r_i, v, \psi_1)$. It should be recognized that, from the symmetry assumptions, $f(r_i, v, \theta) = f(r_i, v, -\theta)$.

IV. NUMERICAL RESULTS

We must now make some assumptions in order to proceed. Specifically, we must define the galactic velocity distribution and the local background density of DM, as well as the nuclear form factor. We use the value $n_\chi = n_{\chi^*} = 0.2 \text{ GeV/cm}^3$, which is half of the local DM density [57–60]. In any example where elastic scattering is considered, we assign n_χ the value 0.4 GeV/cm^3 . We will also assume the standard Maxwellian model for the galactic velocity distribution, with a shift to the solar frame,

$$f(u) = \frac{u}{\sqrt{\pi}v_\odot^2} \left[\exp\left(-\frac{3}{2}\frac{(u-v_\odot)^2}{\bar{v}^2}\right) - \exp\left(-\frac{3}{2}\frac{(u+v_\odot)^2}{\bar{v}^2}\right) \right]. \quad (42)$$

The solar velocity through the Milky Way, v_\odot , is taken to be 220 km/s, and the velocity dispersion $\bar{v} = 270 \text{ km/s}$.

Unless otherwise stated, we use the DM-proton cross section $\sigma_{\chi p} = 10^{-42} \text{ cm}^2$. Both in the case of capture and subsequent scattering of captured particles, we use the Helm form factor [61]

$$F(q) = 3\frac{j_1(qR)}{qR}e^{-q^2s^2/2}, \quad (43)$$

where $q = \sqrt{2m_A E_R}$ is the momentum transfer in the scattering process, j_1 is the spherical Bessel function of the first kind and R is given by

$$R = \sqrt{b^2 + \frac{7}{3}\pi^2 a^2 - 5s^2}. \quad (44)$$

The values we use in the above, $a = 0.52 \text{ fm}$, $s = 0.9 \text{ fm}$, $b = (1.23A^{1/3} - 0.6) \text{ fm}$, are taken from in Ref. [62]. We will only take into account scattering on the elements hydrogen, helium, nitrogen, oxygen, neon and iron with radial abundances taken from the AGSS09ph solar model [63]. This is due to the fact that the abundances of the other solar elements are negligible and contribute very little to scattering rates and some time can be saved when calculating C_α and $\Sigma_{\alpha\beta}$.

We use 100 individual states in E that are uniformly distributed over all possible bound state energies. For every discretization point in E , L is uniformly discretized in 100 states between 0 and L_{\max} , which is the largest allowed angular momentum for the given energy and can be found by inverting Eq. (8). Therefore, in total, we use 10000 states.

The following plots will be shown in units of energy (E) of GM_{\odot}/R_{\odot} , and in units of angular momentum (L) of $\sqrt{GM_{\odot}R_{\odot}}$, where M_{\odot} and R_{\odot} are the solar mass and radius, respectively. One can easily check that these quantities naturally correspond to the typical energy and angular momentum of a DM particle orbiting around the centre of the Sun:

$$E_{\chi} = m_{\chi}E = m_{\chi} \frac{GM_{\odot}}{R_{\odot}} \simeq 20 \left(\frac{m_{\chi}}{10 \text{ GeV}} \right) \text{ keV}, \quad (45)$$

$$L_{\chi} = m_{\chi}L = m_{\chi} \left(\frac{GM_{\odot}}{R_{\odot}} \right)^{1/2} R_{\odot} \simeq 0.03 \left(\frac{m_{\chi}}{10 \text{ GeV}} \right) \text{ GeV s}. \quad (46)$$

Furthermore, notice that $E_{\chi} \sim \delta$ for typical WIMP masses, and therefore it is expected that the excited state can be created by endothermic scatterings (see also the discussions in Refs. [27, 34]).

A. The distribution of captured particles

In Fig. 1, we show the density of capture in E - L space, normalized by its maximum value, for the elastic case, taking the DM mass $m_{\chi} = 5 \text{ GeV}$. Capture is dominated by helium and oxygen, followed by a slightly lower capture rate by hydrogen and nitrogen. The concentration of capture in the region centred slightly above $E = -1$ and $L \sim 0.3$ is due to scattering on hydrogen, which absorbs little recoil energy due to its low mass relative to the DM. For helium, oxygen and nitrogen, capture tends to be concentrated towards more strongly bound orbits, with a preference for more circular orbits, i.e., larger L .

Moving on to inelastic scattering, Fig. 2 shows an example of the density of capture of DM, with capture of χ in the left plot and χ^* in the right plot. We use $m_{\chi} = 100 \text{ GeV}$ and $\delta = 100 \text{ keV}$. The capture rate of χ particles, C_{χ} , is roughly half as large as the capture of χ^* , C_{χ^*} , which is expected from previous studies, see e.g., Ref. [38]. An interesting difference between the capture of χ and χ^* particles is the fact that the former are captured into more tightly bound orbits than the latter. This is due to two reasons, the first of which is that a significant amount of kinetic energy is lost in the endothermic process to produce the χ^* . This loss of energy reduces the form-factor suppression as the momentum transfer is not as large. Scattering takes place primarily on iron which, due to its large mass, is also a superb target for absorbing recoil energy relative to the other elements in this case. On the other hand, energy being released in the exothermic case translates

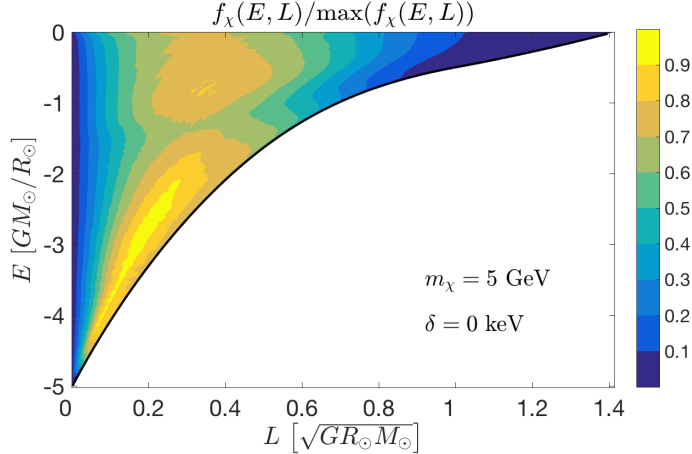


FIG. 1: The density of DM capture, normalized by the largest value of the distribution, in the E - L plane. An elastic cross section is used and the DM mass is set to $m_\chi = 5$ GeV.

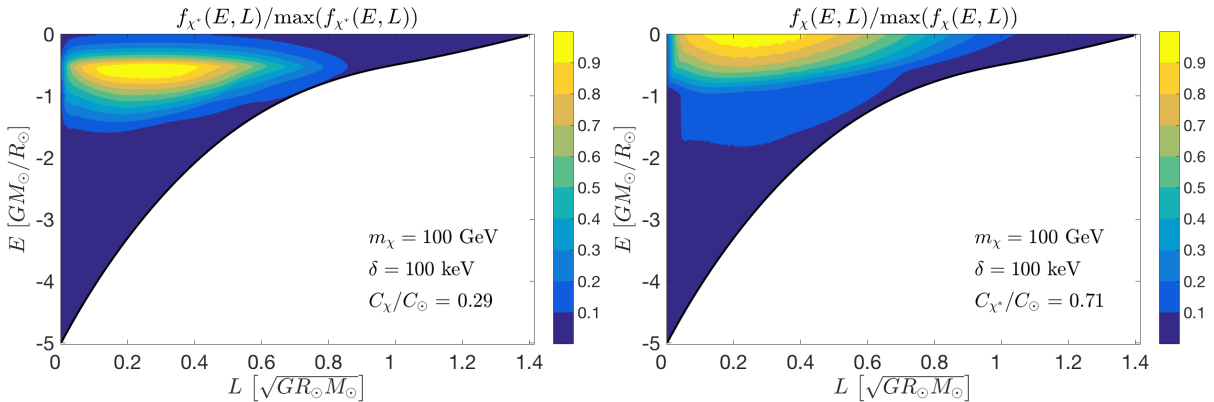


FIG. 2: The density of capture for inelastic DM with $m_\chi = 100$ GeV and $\delta = 100$ keV in the E - L plane. Left: the capture of halo χ particles. Right: the capture of halo χ^* particles. Both distributions are normalized by their own largest value.

into a larger form factor suppression and thus a preference for scattering events in which the DM particle loses as little energy as possible, leaving it less tightly bound. In this case, capture occurs primarily due to scattering with helium nuclei and to a lesser degree with oxygen, both of which are not very efficient at absorbing recoil energy.

B. Time evolution of the distribution in E - L space

Having calculated the $\Sigma_{\alpha\beta}$ matrix, the total scattering rate from every state can be found. The case with $m_\chi = 100$ GeV and $\delta = 100$ keV is shown in Fig. 3, where we plot the base 10 logarithm

of the total scattering rate times the solar lifetime, for $\chi \rightarrow \chi^*$ in the left plot and for $\chi^* \rightarrow \chi$ in the right one.

The largest rate for scattering of $\chi \rightarrow \chi^*$ is found for the states with low angular momentum and medium energy. These are the particles that have enough energy to travel fairly far out from the solar center. When they fall back into the solar center, they regain a significant amount of kinetic energy, which allows endothermic scattering to take place. Particles with larger energies spend more of their time outside the Sun, which decreases their scattering rate. There are also two regions, one at very low energies and one at very high energies and large angular momenta, where scattering does not take place at all. This can be explained by the fact that the total kinetic energy in collisions taking place in most of the E - L plane is supplied almost entirely by the DM particle. The only region where this is not the case is in the very low E region in which DM particle orbits are confined to the solar center. These particles have very low velocities, and the energy of nuclei, even though the temperature is high, is not sufficient to provide conditions in which up-scattering can take place. At large E and large L , the nuclei are essentially stationary and the DM particles will always have low velocities due to their circular orbits, leading to the conclusion that up-scattering is kinematically disallowed also in this region. Even if scattering is allowed, the rates are suppressed due to the DM travelling on orbits in which they spend the vast majority of their time outside the Sun.

The scattering of $\chi^* \rightarrow \chi$ is never suppressed for kinematic reasons since the process is exothermic. The rates are thus largest for particles that are confined to the solar center, i.e., in the low E and L region. The only suppression in the scattering rate comes for states at increasing E which spend more time in less dense regions. The extreme case is thus for very large E and L , with highly circular orbits in the outer regions of the Sun, where the density of targets is the lowest, the DM velocity is small, and most of the time is spent outside the Sun. Interestingly, it can also be seen that the rate for exothermic scattering to take place is larger than the rate for endothermic scattering in the entire $E - L$ plane. This indicates that the form-factor suppression, which is expected to be larger for exothermic scattering, is not as strong as the kinematic suppression of endothermic scattering.

Next, we can take a sample of freshly captured DM particles in a time Δt which is small enough for no additional scattering post capture to have occurred. The time evolution is then found by solving Eq. (11), neglecting additional capture and annihilation, with the initial distribution

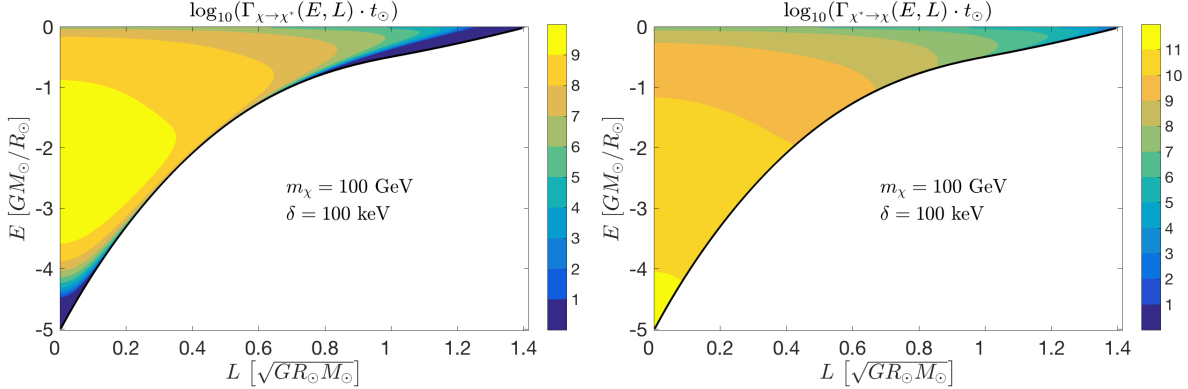


FIG. 3: The base 10 logarithm of the total scattering rates of DM particles with $m_\chi = 100$ GeV and $\delta = 100$ keV times the solar lifetime t_\odot in the E - L plane. Left: Endothermic scattering rate, Right: Exothermic scattering rate.

$\vec{f}(0) = \vec{C}\Delta t$. The distribution will then evolve in time as

$$\vec{f}(t) = e^{\Sigma t} \vec{C}\Delta t. \quad (47)$$

Figure 4 shows the base 10 logarithm of the distribution at various times for $m_\chi = 5$ GeV. The distribution accumulates into the lower region of the E - L space very rapidly. Taking the scale into account, the distribution comes close to equilibrium at $t \sim 10^{-7} t_\odot$, at which point most particles in the Sun have gathered in orbits with very low energies. As time evolves further, there is a constant flow from the few remaining particles at larger E down towards the lower energy orbits. It is also interesting to note that the evaporation is negligible over a solar lifetime, i.e., $N_\chi(t_\odot)/N_\chi(0) = 1$.⁵

We now use Eq. (36) to translate the distribution in E - L space into a radial distribution. The results for elastic scattering are shown in Fig. 5 for the times $t = 10^{-10} t_\odot$ (left), $t = 10^{-8} t_\odot$ (middle) and $t = 10^{-6} t_\odot$ (right). The distribution is compared to the isothermal one of Eq. (33), with the angular degrees of freedom integrated over. One can see that the distribution has essentially reached equilibrium already at $t = 10^{-8} t_\odot$, changing only slightly at $t = 10^{-6} t_\odot$. The Boltzmann distribution gives a fairly accurate description of the distribution, although the numerically computed one is slightly shifted towards larger radii, and its peak is not as pronounced.

Moving on to the case of inelastic DM, we will again focus our discussion on the illustrative case of $m_\chi = 100$ GeV and $\delta = 100$ keV. Figure 6 shows the base 10 logarithm of the χ (χ^*) distribution in the E - L plane in the left (right) plot at various times. As in the case of elastic

⁵ The figure at $t = t_\odot$ is in good agreement with Fig. 3.1 in Ref. [51].

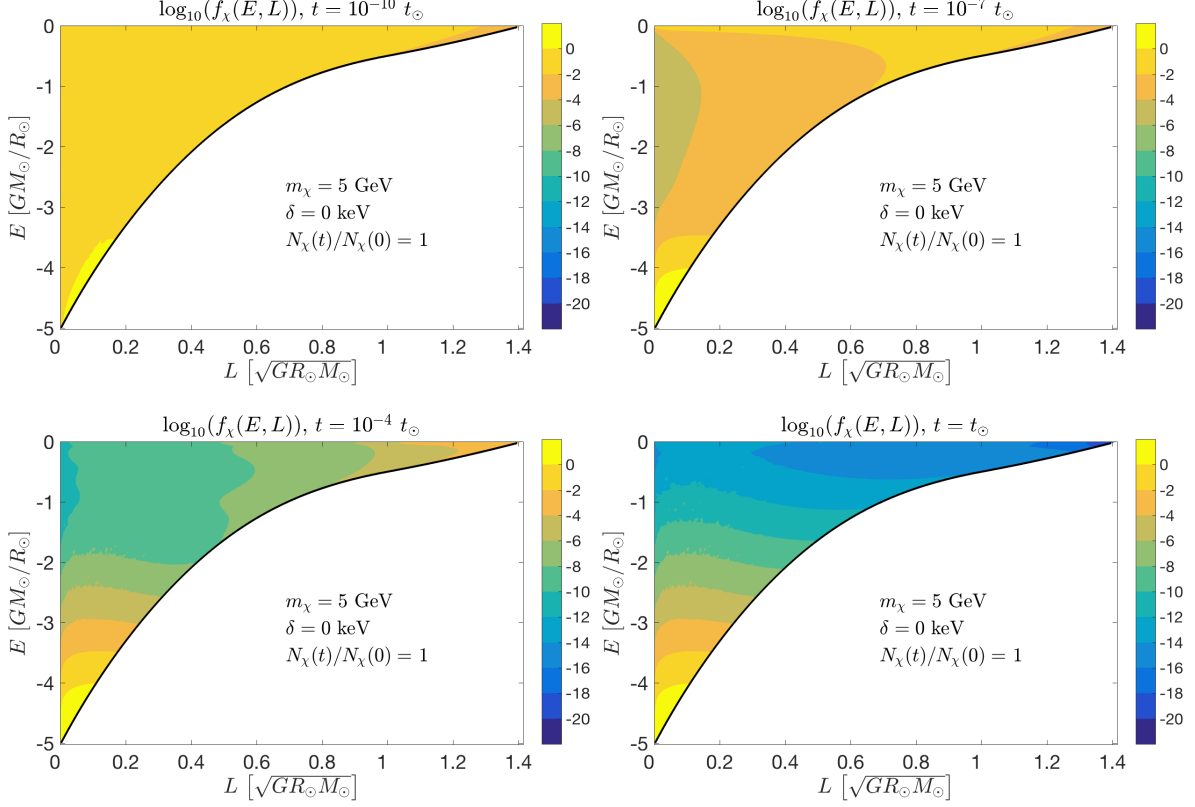


FIG. 4: The base 10 logarithm of the distribution of elastic DM at various times, with an initial distribution $\vec{f}(0) = \vec{C} \Delta t$. The DM mass is set to $m_\chi = 5$ GeV.

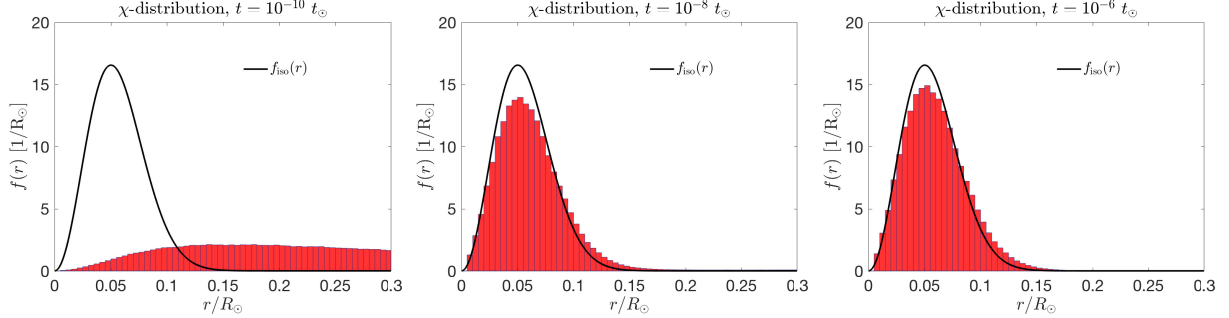


FIG. 5: The radial distribution of elastic DM at times $t = 10^{-10} t_\odot$ (left), $t = 10^{-8} t_\odot$ (middle) and $t = 10^{-6} t_\odot$ (right), for $m_\chi = 5$ GeV.

scattering, the distribution of χ concentrates in the low E region very quickly. It is also apparent that the contribution from χ^* to the total number of DM particles rapidly becomes negligible. At later times, χ^* will only appear from regions where χ has an extremely small scattering rate, i.e., from the large E and large L region, and from the very low E region, see Fig. 3. These are the two regions in which a substantial population of χ appears as well. However, the former region

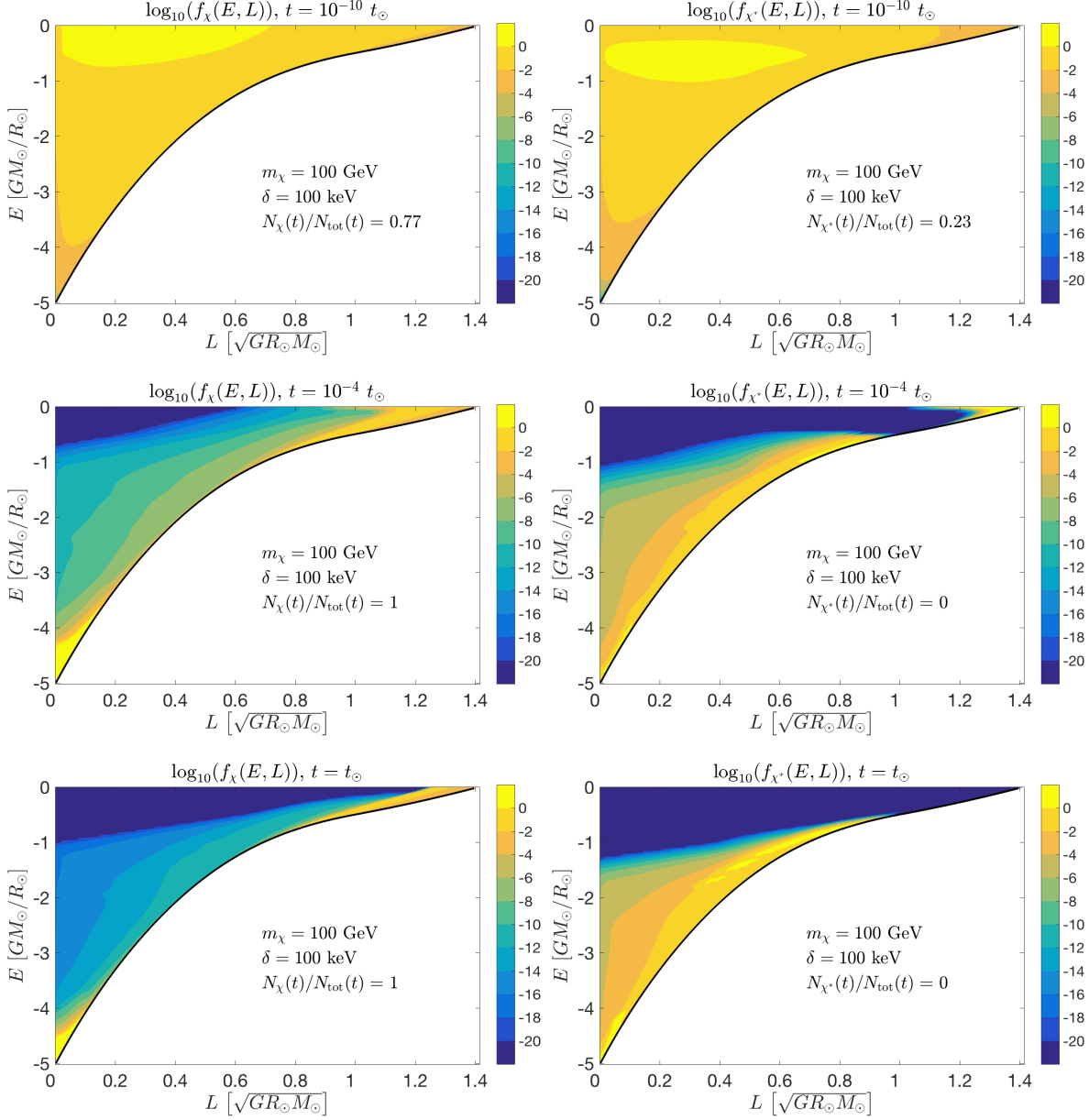


FIG. 6: The base 10 logarithm of the distribution of DM at various times, with an initial distribution given by the capture rate. We use $m_\chi = 100$ GeV and $\delta = 100$ keV. The left column shows the χ distribution, and the right column shows the χ^* distribution.

will mainly be occupied by particles that were captured into it, as the majority of particles that scatter after being captured will find themselves at significantly lower E .⁶ It is easy to justify the behaviour of the distribution at large times: one expects the number of χ^* to be absolutely negligible as χ particles end up in orbits where the rate of up-scattering is extremely small and the

⁶ This is not clear from Fig. 2 due to the scaling. It can however be seen in Fig. 6 at $t = 10^{-10}t_\odot$.

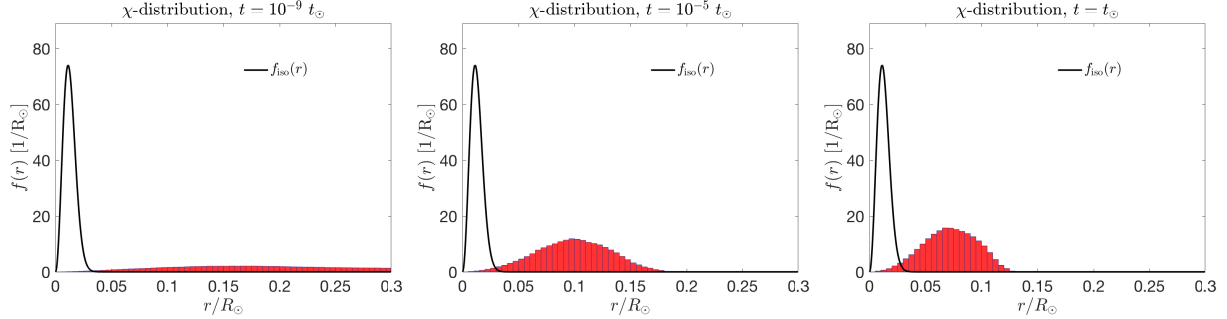


FIG. 7: The radial distribution of χ particles, $f_{\text{num}}(r)$, at various times $t = 10^{-9} t_{\odot}$ (left), $t = 10^{-5} t_{\odot}$ (middle) and $t = t_{\odot}$ (right). We use $m_{\chi} = 100$ GeV and $\delta = 100$ keV.

few particles that up-scatter will down-scatter almost immediately (the regions at low E , and at large E and L , in Fig. 3.)

Finally, we obtain the radial distributions for inelastic scattering. The results are shown in Fig. 7. At very early times, the distribution extends up to large radii. At $t = 10^{-9} t_{\odot}$, a large concentration starts to form, shown below $r/R_{\odot} \simeq 0.3$, that very slowly moves towards lower radii, forming a distribution centred at $r/R_{\odot} \simeq 0.1$ at $t = 10^{-5} t_{\odot}$. However, even at $t = t_{\odot}$, the distribution has not reached a stationary state. Another important observation is that the Boltzmann distribution is now a very poor description of the final distribution. This is entirely due to particles being trapped with no possibility of scattering further, in particular those in the region at low E which are the ones that contribute to $f_{\text{num}}(r)$ at smaller radii. Since the number of χ^* particles is completely negligible, the total DM distribution is identical to the χ distribution.

C. Annihilation and evaporation

In order to investigate the effects that the altered distribution will have on the annihilation rate, we use Eq. (38) to calculate the number of particles at $t = t_{\odot}$. This distribution contains information on the total number of particles in the Sun, and therefore it provides a more realistic distribution. In fact, sets of particles that are captured at different times will be distributed differently in the Sun at $t = t_{\odot}$, and thus will contribute differently to the overall distribution. Of course, the number of particles that has evaporated will also be affected by the amount of time that passed since they were originally captured.

We now calculate distributions of inelastic DM at $t = t_{\odot}$ for different masses and cross sections

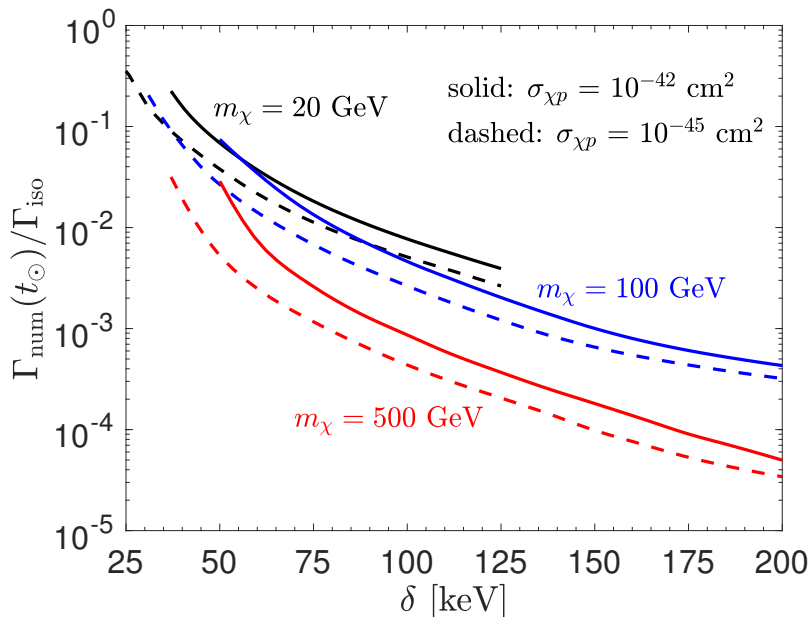


FIG. 8: The suppression of the annihilation rate for the numerically calculated distribution relative to the isothermal distribution using $\sigma_{\chi p} = 10^{-42}$ cm² (solid lines) and $\sigma_{\chi p} = 10^{-45}$ cm² (dashed lines). The colors indicate DM masses: $m_{\chi} = 20$ GeV (black), $m_{\chi} = 100$ GeV (blue) and $m_{\chi} = 500$ GeV (red).

and show in Fig. 8 the ratio of the numerically calculated annihilation rate to the isothermal one, computed using Eq. (41), as a function of δ .⁷ The results are shown for two scattering cross sections: $\sigma_{\chi p} = 10^{-42}$ cm² (solid lines) and $\sigma_{\chi p} = 10^{-45}$ cm² (dashed lines), and for three different DM masses: $m_{\chi} = 20$ GeV (black lines), $m_{\chi} = 100$ GeV (blue lines), and $m_{\chi} = 500$ GeV (red lines). The annihilation rate is severely suppressed for large values of δ , the reason being that as δ increases, so do the regions in which additional scattering of χ is kinetically forbidden, which in turn leads to a more diluted DM distribution. The fact that the distribution does not reach a steady state within a solar lifetime is apparent when considering cases with different scattering cross sections (which is equivalent to considering different times), as the suppression for $\sigma_{\chi p} = 10^{-42}$ cm² is not as severe as the one for $\sigma_{\chi p} = 10^{-45}$ cm². Note that the number of captured particles depends on the scattering cross section. However, N drops in the ratio $\Gamma_{\text{num}}(t_{\odot})/\Gamma_{\text{iso}}$ and therefore the larger ratio for the larger scattering cross section is not due to the total number of DM particles, but to their different distributions.

⁷ Note that the distribution (needed to calculate the annihilation rate) cannot be determined with a good accuracy for values of δ that are smaller than those shown in Fig. 8. The reason for this is that in these cases the distributions are limited to the central region of the Sun, and our discretization in E is not fine enough to find the radial distribution, as nearly all particles would occupy the very lowest energy states.

Next, we use the number density distributions, computed with the same parameters as before, to calculate the actual annihilation rate using Eq. (40), where we assume s-wave annihilation and assign the thermal averaged cross section the value $\langle\sigma_{\text{ann}}v\rangle = 3 \cdot 10^{-26} \text{ cm}^3/\text{s}$. The results are shown in Fig. 9, where the annihilation rates (solid lines) are compared to the solar capture rates (dashed lines). We only show the results for $\sigma_{\chi p} = 10^{-42} \text{ cm}^2$, keeping in mind that the annihilation rate is substantially lower the smaller the scattering cross section. Only in the cases of $m_\chi = 20 \text{ GeV}$ and $m_\chi = 100 \text{ GeV}$ does the annihilation rate exceed the capture rate for the ranges in δ for which we can obtain accurate radial distributions. The general trend is that the annihilation rate increases with a decreasing δ , i.e., when we approach the elastic limit. One should keep in mind that what is presented here is an upper limit on the annihilation rate rather than the actual annihilation rate, since we neglected annihilations when computing the distributions. Adding annihilations would reduce the total number of particles at any given time, which would in turn reduce the annihilation rate. On the other hand, as already mentioned, a non-spherically symmetric distribution with the same number of particles would increase the annihilation rate. It is thus unclear whether equilibrium between DM capture and annihilation is reached if the capture rate is similar in magnitude but slightly lower than Γ_{num} , as is the case for very small δ . If, however, Γ_{num} is lower than the solar capture rate (which is itself an upper bound on the annihilation rate), equilibrium has not occurred. This is the case for most values of δ in Fig. 9. An exception for the latter statement is if there is a significant angular dependence in the final distribution which would boost the annihilation rate.

Finally, we are interested in knowing how much evaporation affects the total number of DM particles. In the elastic case, it is generally accepted that DM particles with masses below $m_\chi \sim 3 - 4 \text{ GeV}$ will evaporate before being able to annihilate after they are captured. The situation is not at all as clear in the case of inelastic DM, due to the absorption and release of energy as the DM particle scatters back and forth between the heavier and lighter states. Evaporation is thus a cause for concern, in particular for sizeable δ .

In Fig. 10 we show the total number of particles $N(t_\odot)$ in the Sun at $t = t_\odot$ divided by its initial value $N(0)$. $N(t)$ is calculated using Eq. (47), again for different DM masses: $m_\chi = 20 \text{ GeV}$ (black line), $m_\chi = 100 \text{ GeV}$ (red line) and $m_\chi = 500 \text{ GeV}$ (blue line). One can see that there is a value of the splitting $\delta_{\text{max}}(m_\chi)$ where the evaporation rate reaches a maximum. This value increases with the DM mass. For a given DM mass, at splittings much smaller or much larger than δ_{max} , the evaporation rate vanishes, or becomes negligible. The former case, $\delta \ll \delta_{\text{max}}$ is well-known, as it corresponds to the elastic limit, where evaporation is important only for very low DM masses

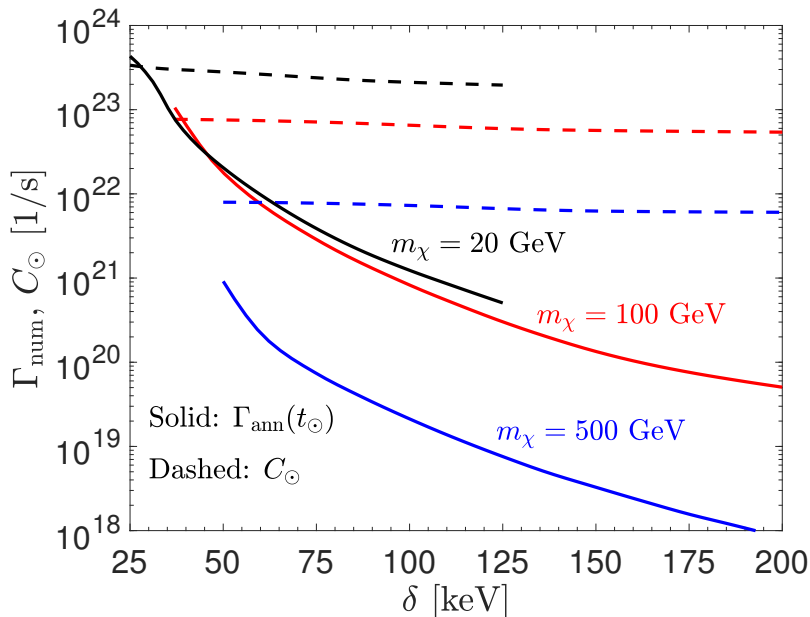


FIG. 9: Comparison between the annihilation rate (solid lines) with the capture rate (dashed lines) for the numerically calculated distributions. We use $\sigma_{\chi p} = 10^{-42} \text{ cm}^2$, $\langle \sigma_{\text{ann}} v \rangle = 3 \cdot 10^{-26} \text{ cm}^3/\text{s}$, and three different DM masses: $m_\chi = 20 \text{ GeV}$ (black), $m_\chi = 100 \text{ GeV}$ (red) and $m_\chi = 500 \text{ GeV}$ (blue).

($m_\chi \sim 3 - 4 \text{ GeV}$). For the latter case, $\delta \gg \delta_{\text{max}}$, evaporation becomes suppressed due to two reasons. First, halo χ particles are captured into states with, on average, lower E as δ is increased, which reduces the likeliness that the particle evaporates as it subsequently transitions into the lower state. Halo χ^* are captured into high E states, but as these particles scatter back into χ^* for the first time since they were captured, it is extremely likely that they drop to a significantly lower E state which inhibits their evaporation. Second, the χ scatterings may not be kinematically allowed, and if they are, the resulting χ^* end up with very little energy, and therefore in strongly bound orbits. As can be observed, the evaporation rate is extremely low over a solar lifetime, where at most 1 (2) % percent of particles have evaporated over the solar lifetime for $m_\chi \lesssim 100$ (500) GeV.

V. SUMMARY AND CONCLUSIONS

In this paper we have studied the evolution of the distribution of inelastic DM in the Sun. We have presented the results of a numerical simulation of the process of DM capture and further scattering with nuclei in the Sun. We were particularly interested in the case of inelastic DM with splittings δ ranging from tens to hundreds of keV.

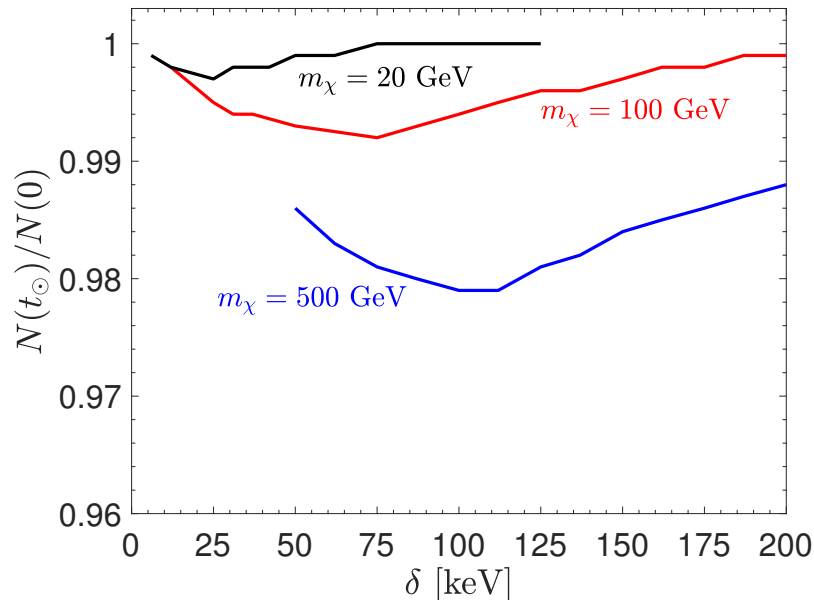


FIG. 10: The ratio between the total number of particles, after the distribution has been evolved for a solar lifetime, and the initial number of particles. The DM masses are $m_\chi = 20$ GeV (black), $m_\chi = 100$ GeV (red) and $m_\chi = 500$ GeV (blue).

Our goal was to quantitatively study the process of thermalization. In order for our simulation to be computationally feasible, we have neglected annihilations in the evolution equation. For definiteness, we have assumed that the DM halo consists of equal populations of the two different states.⁸ Taking some initially captured distributions of χ and χ^* , we have evolved them in order to study the final distributions at a time equal to the solar lifetime. We have found that χ^* are absent in the final distribution, see Fig. 6. We found a χ -distribution that has not reached a stationary state at a solar lifetime, and that is far from being isothermal (Maxwell-Boltzmann) with a temperature equal to that of the solar core, see Fig. 7, unlike in the case of elastic scattering (c.f. Fig. 4).

By assuming spherical symmetry, we have also computed an upper bound on the annihilation rate and found that it is quite suppressed for splittings larger than a few tens of keV. The exact suppression factor depends on the DM mass and the scattering rate, see Fig. 8, but it is quite robust to state that, for mass splittings above roughly 50 keV, unless deviations from spherical symmetry in the distribution are present, the annihilation rate may be too small to yield a large

⁸ We defer the case in which χ^* is unstable, and the case of light mediators, for future work.

enough neutrino rate to be observable at Earth based neutrino telescopes.

Similarly, by comparing the numerically obtained annihilation rates to the case where annihilations are given by the capture rates, which is the exact limit in which evaporation is negligible and when equilibrium has been reached (see dashed lines in Fig. 9), we have found that equilibrium is not reached unless the splittings are below roughly 50 keV. For the DM masses considered, equilibrium is achieved at values of $\delta(\text{keV})/m_\chi(\text{GeV})$ equal or smaller than a few. Interestingly, the larger the DM masses, the greater the slopes of the annihilation rates (solid lines), and therefore it is expected that there is a maximum splitting δ , for equilibration to occur, that is independent of the DM mass. We have also studied evaporation, and found that it plays a less important role than previously thought of, staying safely below a few percent for the splittings and DM masses considered, c.f. Fig. (10).

The most phenomenologically relevant implications of this work are regarding the detection of neutrinos from DM annihilations in the Sun. The most promising cases to have a large annihilation rate are those where a non-negligible elastic cross section is also present or in the case of very small mass splittings ($\lesssim \mathcal{O}(10)$ keV).

We would finally like to point out that it would also be interesting to pursue numerical studies of scenarios with large DM self-interactions, which would contribute to both capture and evaporation, in which case one could also incorporate DM annihilations for the same prize.

Acknowledgements

We would like to thank Sergio Palomares-Ruiz for useful discussions and Simon Velander for participation during the early stages of this project. The authors acknowledge the support from the Spanish MINECO through the “Ramón y Cajal” programme (RYC-2015-18132) and through the Centro de Excelencia Severo Ochoa Program under grant SEV-2016-0597 [M.B.], the Göran Gustafsson foundation [M.B., S.C.], and the Australian Research Council through the ARC Centre of Excellence for Particle Physics at the Terascale (CoEPP) (CE110001104) [J.H.-G.]. S.C. also acknowledges the hospitality of Instituto de Física Teórica (IFT) and the support from the Roland Gustafsson foundation for theoretical physics during his stay at IFT as part of this work was carried out.

[1] L. Bergström, Rept. Prog. Phys. **63**, 793 (2000), hep-ph/0002126.

[2] G. Bertone, D. Hooper, and J. Silk, Phys. Rept. **405**, 279 (2005), hep-ph/0404175.

- [3] J. L. Feng, *Ann. Rev. Astron. Astrophys.* **48**, 495 (2010), 1003.0904.
- [4] G. Bertone and D. Hooper, Submitted to: *Rev. Mod. Phys.* (2016), 1605.04909.
- [5] W. H. Press and D. N. Spergel, *Astrophys. J.* **296**, 679 (1985).
- [6] K. Griest and D. Seckel, *Nucl. Phys.* **B283**, 681 (1987), [Erratum: *Nucl. Phys.*B296,1034(1988)].
- [7] A. Gould, *Astrophys. J.* **321**, 571 (1987).
- [8] A. D. Avrorin et al. (Baikal), *Astropart. Phys.* **62**, 12 (2015), 1405.3551.
- [9] K. Choi et al. (Super-Kamiokande), *Phys. Rev. Lett.* **114**, 141301 (2015), 1503.04858.
- [10] M. G. Aartsen et al. (IceCube), *Eur. Phys. J.* **C77**, 146 (2017), 1612.05949.
- [11] A. Albert et al. (ANTARES), *Phys. Dark Univ.* **16**, 41 (2017), 1612.06792.
- [12] D. N. Spergel and W. H. Press, *Astrophys. J.* **294**, 663 (1985).
- [13] I. P. Lopes, J. Silk, and S. H. Hansen, *Mon. Not. Roy. Astron. Soc.* **331**, 361 (2002), astro-ph/0111530.
- [14] A. Bottino, G. Fiorentini, N. Fornengo, B. Ricci, S. Scopel, and F. L. Villante, *Phys. Rev.* **D66**, 053005 (2002), hep-ph/0206211.
- [15] M. T. Frandsen and S. Sarkar, *Phys. Rev. Lett.* **105**, 011301 (2010), 1003.4505.
- [16] M. Taoso, F. Iocco, G. Meynet, G. Bertone, and P. Eggenberger, *Phys. Rev.* **D82**, 083509 (2010), 1005.5711.
- [17] D. T. Cumberbatch, J. Guzik, J. Silk, L. S. Watson, and S. M. West, *Phys. Rev.* **D82**, 103503 (2010), 1005.5102.
- [18] I. Lopes and J. Silk, *Astrophys. J.* **757**, 130 (2012), 1209.3631.
- [19] I. Lopes, K. Kadota, and J. Silk, *Astrophys. J. Lett.* **780**, L15 (2014), 1310.0673.
- [20] I. Lopes, P. Panci, and J. Silk, *Astrophys. J.* **795**, 162 (2014), 1402.0682.
- [21] A. C. Vincent, P. Scott, and A. Serenelli, *Phys. Rev. Lett.* **114**, 081302 (2015), 1411.6626.
- [22] M. Blennow and S. Clementz, *JCAP* **1508**, 036 (2015), 1504.05813.
- [23] A. C. Vincent, A. Serenelli, and P. Scott, *JCAP* **1508**, 040 (2015), 1504.04378.
- [24] C.-S. Chen, G.-L. Lin, and Y.-H. Lin, *Phys. Dark Univ.* **14**, 35 (2016), 1508.05263.
- [25] A. C. Vincent, P. Scott, and A. Serenelli, *JCAP* **1611**, 007 (2016), 1605.06502.
- [26] B. Geytenbeek, S. Rao, P. Scott, A. Serenelli, A. C. Vincent, M. White, and A. G. Williams, *JCAP* **1703**, 029 (2017), 1610.06737.
- [27] D. Tucker-Smith and N. Weiner, *Phys. Rev.* **D64**, 043502 (2001), hep-ph/0101138.
- [28] R. Bernabei et al. (DAMA, LIBRA), *Eur. Phys. J.* **C67**, 39 (2010), 1002.1028.
- [29] R. Abusaidi et al. (CDMS), *Phys. Rev. Lett.* **84**, 5699 (2000), astro-ph/0002471.
- [30] D. S. Akerib et al. (LUX), *Phys. Rev. Lett.* **118**, 021303 (2017), 1608.07648.
- [31] X. Cui et al. (PandaX-II), *Phys. Rev. Lett.* **119**, 181302 (2017), 1708.06917.
- [32] E. Aprile et al. (XENON), *Phys. Rev. Lett.* **119**, 181301 (2017), 1705.06655.
- [33] N. Bozorgnia, J. Herrero-Garcia, T. Schwetz, and J. Zupan, *JCAP* **1307**, 049 (2013), 1305.3575.
- [34] S. Nussinov, L.-T. Wang, and I. Yavin, *JCAP* **0908**, 037 (2009), 0905.1333.
- [35] A. Menon, R. Morris, A. Pierce, and N. Weiner, *Phys. Rev.* **D82**, 015011 (2010), 0905.1847.

- [36] J. Shu, P.-f. Yin, and S.-h. Zhu, *Phys. Rev.* **D81**, 123519 (2010), 1001.1076.
- [37] M. McCullough and L. Randall, *JCAP* **1310**, 058 (2013), 1307.4095.
- [38] M. Blennow, S. Clementz, and J. Herrero-Garcia, *JCAP* **1604**, 004 (2016), 1512.03317.
- [39] J. Smolinsky and P. Tanedo, *Phys. Rev.* **D95**, 075015 (2017), 1701.03168.
- [40] M. McCullough and M. Fairbairn, *Phys. Rev.* **D81**, 083520 (2010), 1001.2737.
- [41] D. Hooper, D. Spolyar, A. Vallinotto, and N. Y. Gnedin, *Phys. Rev.* **D81**, 103531 (2010), 1002.0005.
- [42] M. Baryakhtar, J. Bramante, S. W. Li, T. Linden, and N. Raj, *Phys. Rev. Lett.* **119**, 131801 (2017), 1704.01577.
- [43] K. Schutz and T. R. Slatyer, *JCAP* **1501**, 021 (2015), 1409.2867.
- [44] Y. Zhang, *Phys. Dark Univ.* **15**, 82 (2017), 1611.03492.
- [45] M. Blennow, S. Clementz, and J. Herrero-Garcia, *JCAP* **1703**, 048 (2017), 1612.06681.
- [46] L. J. Hall, T. Moroi, and H. Murayama, *Phys. Lett.* **B424**, 305 (1998), hep-ph/9712515.
- [47] Y. Cui, D. E. Morrissey, D. Poland, and L. Randall, *JHEP* **05**, 076 (2009), 0901.0557.
- [48] S. Chang, N. Weiner, and I. Yavin, *Phys. Rev.* **D82**, 125011 (2010), 1007.4200.
- [49] J. Bramante, P. J. Fox, G. D. Kribs, and A. Martin, *Phys. Rev.* **D94**, 115026 (2016), 1608.02662.
- [50] A. Gould, *Astrophys. J.* **321**, 560 (1987).
- [51] Z.-L. Liang, Y.-L. Wu, Z.-Q. Yang, and Y.-F. Zhou, *JCAP* **1609**, 018 (2016), 1606.02157.
- [52] A. R. Zentner, *Phys. Rev.* **D80**, 063501 (2009), 0907.3448.
- [53] J. Faulkner and R. L. Gilliland, *Astrophys. J.* **299**, 994 (1985).
- [54] R. Garani and S. Palomares-Ruiz, *JCAP* **1705**, 007 (2017), 1702.02768.
- [55] M. Nauenberg, *Phys. Rev.* **D36**, 1080 (1987).
- [56] A. Widmark, *JCAP* **1705**, 046 (2017), 1703.06878.
- [57] R. Catena and P. Ullio, *JCAP* **1008**, 004 (2010), 0907.0018.
- [58] J. I. Read, *J. Phys.* **G41**, 063101 (2014), 1404.1938.
- [59] M. Pato, F. Iocco, and G. Bertone, *JCAP* **1512**, 001 (2015), 1504.06324.
- [60] S. Sivertsson, H. Silverwood, J. I. Read, G. Bertone, and P. Steger, Submitted to: *Mon. Not. Roy. Astron. Soc.* (2017), 1708.07836.
- [61] R. H. Helm, *Phys. Rev.* **104**, 1466 (1956).
- [62] J. D. Lewin and P. F. Smith, *Astropart. Phys.* **6**, 87 (1996).
- [63] A. Serenelli, S. Basu, J. W. Ferguson, and M. Asplund, *Astrophys. J.* **705**, L123 (2009), 0909.2668.